Experimental results from heavy ion collisions

Jana Bielčíková[a,b,*]

[a] *Nuclear Physics Institute of the Czech Academy of Sciences,*
Hlavní 130, 250 68 Řež, Czech Republic

[b] *Faculty of Nuclear Sciences and Physical Engineering, Czech Technical University in Prague,*
Břehová 7, 115 19 Praha, Czech Republic

E-mail: bielcikova@ujf.cas.cz

In this proceedings, an overview of selected experimental results in heavy-ion collisions focusing on measurements at high energy frontier that explores the high temperature and low baryochemical potential part of the QCD phase diagram is presented. Due to the space limitations only a few prominent results can be highlighted here with a primary focus on hard probes studies with heavy-flavor particles, jets, and quarkonia measured by the experiments at the LHC CERN and RHIC at BNL. The interested reader is therefore kindly referred to the individual contributions at the conference.

41st International Conference on High Energy physics - ICHEP2022
6-13 July, 2022
Bologna, Italy

*Speaker

Heavy-ion collisions offer a unique way to study properties of strongly interacting matter and its phase diagram in laboratory. At high energy densities, QCD predicts a phase transition from a hadron gas to a deconfined partonic state, the quark-gluon plasma (QGP). QCD calculations on a lattice have established that this transition is a crossover at the temperature $T \approx 154$ MeV for baryochemical potential $\mu_B = 0$. A first-order phase transition and the existence of a critical point at high μ_B is expected and is a subject of an intense search in a dedicated Beam Energy Scan (BES) program at RHIC at BNL [1]. In the following we focus on some of the key observables related to QGP studies at high temperature and low μ_B at the LHC and top RHIC energies.

1. Small collision systems: constraining nPDFs

Small collision systems such as p-Pb or high-multiplicity pp collisions have attracted recently a lot of attention to search for onset of QGP signatures or to constrain parton distribution functions (PDF) in cold nuclear matter. Recent global analyses of nPDFs greatly benefit from the wealth of high precision LHC p-Pb data covering large kinematic region in rapidity and transverse momentum (p_T) including also heavy quarks and quarkonia that allow to study very low values of the parton momentum fraction (x) in nuclei. As an example, let us highlight here the LHCb measurements of charged particles shown in Figure 1 [2] and of π^0s [3] in pp and p-Pb collisions at $\sqrt{s_{NN}} = 5$ TeV. The observed suppression of particle production at forward pseudorapidity (η) and an enhancement in the backward region for $p_T > 1.5$ GeV/c sets significant constrains on nuclear PDFs and saturation models down to $x \approx 10^{-6}$. Recent color glass condensate (CGC) calculations with improved threshold resummation [4], extend the applicability regime of the CGC NLO calculation and enable to quantitatively understand the transition from the CGC to the dilute regime and are able to describe existing LHC and RHIC data across all p_T that has not been possible earlier. The LHCb data on D^0 meson production in p-Pb collisions [5] brought this year a significant improvement in determination of a new nPDF set (nNNPDF3.0) [6]. Within the nCTEQ approach, the new nCTEQ15HQ fit, that includes recent heavy-quark and quarkonia data, constrains the gluon density down to $x = 10^{-5}$ with an uncertainty that is almost an order of magnitude smaller than in previous global fits [7].
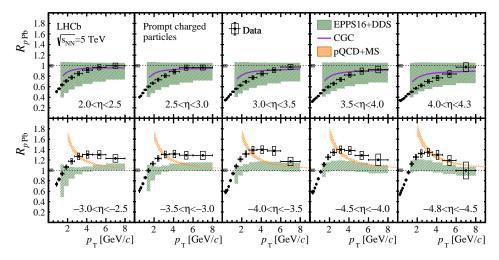

Figure 1: Nuclear modification factor as a function of p_T in different η intervals for the (top) forward and (bottom) backward regions, compared with the predictions. Figure taken from [2].
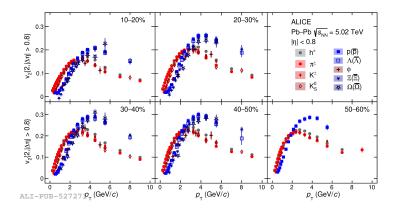
Figure 2: Transverse momentum dependence of v_2 for different particle species measured in Pb-Pb collisions at $\sqrt{s_{NN}} = 5.02$ TeV by ALICE. Figure taken from [8].

2. Collective anisotropic flow

The QGP dynamics can be studied via azimuthal distributions ("flow") of produced particles relative to the reaction plane, that are characterized by the Fourier coefficients (v_n). In particular, the second (v_2) and third (v_3) Fourier coefficients are intensively studied as they are sensitive to the initial collision geometry and event-by-event fluctuations, respectively. Below we highlight recent measurements of the elliptic flow v_2.

In hydrodynamical models, v_2 should depend on the particle mass in the kinematic regime applicable for hydrodynamical description ($p_T < 2$ GeV/c) and is predicted to be larger for lighter particles. Figure 2 displays the p_T dependence of v_2 determined from two-particle correlations at $\sqrt{s_{NN}} = 5.02$ TeV for various identified hadron species. Similar measurement is shown in the left panel of Figure 3 at $\sqrt{s_{NN}} = 19.6$ GeV using the high-statistics BES-II data from STAR. Despite the large span in collision energies, a clear mass ordering pattern for $p_T < 1.5$ GeV/c is observed, in line with hydrodynamical predictions. At higher p_T, particle-type separation, which depends on the valence quark content of the particle, is manifested, indicating that the flow develops on the quark level. Interestingly, similar pattern is also present in small collision system such as p-Pb collisions as displayed in Figure 3 or high-multiplicity pp collisions. The similarities between large and small systems hint to a possible creation of a droplet of QGP in high-multiplicity small collision systems.
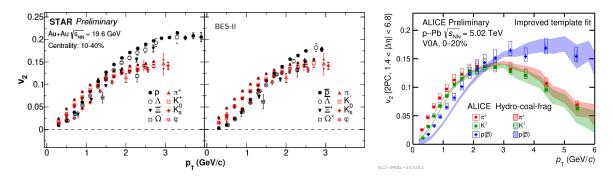

Figure 3: Transverse momentum dependence of v_2 for different particle species measured at $\sqrt{s_{NN}} = 19.6$ GeV by STAR [9] and in p-Pb collisions at $\sqrt{s_{NN}} = 5.02$ TeV by ALICE [10].
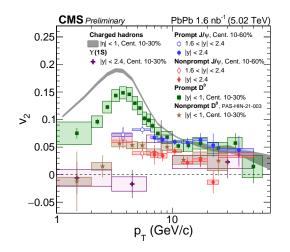
3

Figure 4: Elliptic flow anisotropy v_2 for prompt (circles) and nonprompt J/ψ (diamonds), prompt (squares) and nonprompt D^0 mesons (stars), $\Upsilon(1S)$ (crosses), and charged hadrons (gray band) measured with CMS at $\sqrt{s_{NN}} = 5.02$ TeV [11].

Finally, let us have a look to what extent are heavy-quarks subject to collective effects. Figure 4 displays collection of v_2 measurements for particles containing heavy, c and b quarks. As can be seen, a sizable v_2 is observed for prompt D^0 and J/ψ mesons. The nonprompt D^0 and J/ψ v_2 values are somewhat smaller, suggesting different in-medium effects for c and b quarks. For bottomonia, v_2 is found to be consistent with zero within large uncertainties.

3. Tomography of QGP with hard probes

Experimental studies of QGP are challenging due to its very short lifetime and require in-situ probes created early in the collision and experiencing the whole evolution of the medium. For this purpose, heavy quarks and jets, the so called hard probes, that originate from initial hard scattering of partons and carry a color charge, are commonly used and discussed below.

Before trying to understand QGP, it is first essential to check how well we understand hard probes production in small collision systems as these form a reference baseline for AA collisions. Recent measurements of prompt charm-baryon production in small collision systems show baryon-to-meson yield ratios significantly higher than those in e^+e^- or ep collisions at HERA and Belle, suggesting that the charm fragmentation is not universal across different collision systems. The
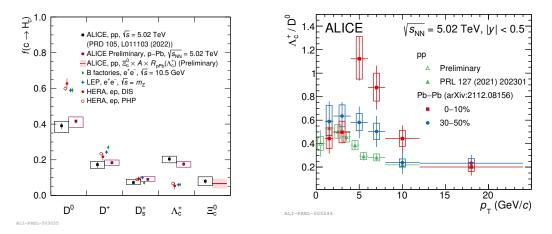

Figure 5: (Left) Fragmentation fractions of prompt charm hadrons in pp and p-Pb collisions at $\sqrt{s_{NN}} = 5.02$ TeV. (Right) Λ_c/D^0 ratio in pp and Pb-Pb collisions at $\sqrt{s_{NN}} = 5.02$ TeV. Figures from [12].
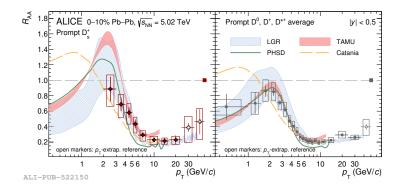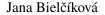
ALI-PUB-522150

Figure 6: The R_{AA} of prompt D meson species in Pb-Pb collisions at $\sqrt{s_{NN}}$ = 5.02 TeV measured by ALICE. Figure taken from [13].

charm fragmentation fraction that represents the probability of a c quark hadronizing into a given charm hadron is Figure 5 (left). In pp and p-Pb collisions, c quarks are found to hadronize into baryons in almost 40%, four times more often than in e^+e^- collisions. The presence of QGP brings additional dynamics into c quark hadronization as corroborated by measurements of Λ_c/D^0 production, where at intermediate p_T a pronounced enhancement relative to pp is present from RHIC [14] to the LHC as demonstrated in Figure 5 (right). This enhacement is similar to that observed for light-flavor hadrons and parton recombination is thus at play also for c quarks.

To quantify the effects of the QGP on particle production, commonly the nuclear modification factor, R_{AA}, defined as the ratio of the observed yield in heavy-ion (AA) collisions to the expectation from an equivalent number of pp collisions, where medium effects from the QGP formation are absent, is used. Parton energy loss in the QGP is expected to follow a hierarchy ordered by parton color charge and mass, with gluons losing more energy than light and heavy quarks. This in turn means, that the in-medium parton energy loss can be used to quantify QGP properties. As demonstrated in Figure 6, the R_{AA} of prompt D mesons is strongly suppressed and similar observations has been also made for Λ_c R_{AA} [15], albeit with larger uncertainties. Models (TAMU, MC@sHQ, LIDO, LGR, and Catania) incorporating charm quark transport and hadronization via recombination and enhanced s quark content in QGP describe the data well, including the R_{AA} of D_s^+ and Λ_c. However, we note that simultaneous description of R_{AA} and v_2 is challenging for the models. Due to interplay of radiative energy loss at higher p_T and recombination at lower p_T D mesons acquire additional flow via charm and light quark recombination. Using the R_{AA}, v_2, and also v_3 measurements of non-strange D mesons, the spatial diffusion coefficient can be constrained to a value of $1.5 < 2\pi D_s T_c < 4.5$ corresponding to a charm relaxation time of $\approx$ 3-8 fm/c at T_c = 155 MeV.

Production of b quarks can be assessed via studies of non-prompt D^0 mesons from beauty-hadron decays. ALICE measured for the first time production of non-prompt D^0 mesons down to p_T = 1 GeV/c, significantly extending the previous CMS measurement. Figure 7 shows, the R_{AA} ratio of non-propmt and prompt D^0 and v_2 of non-prompt D^0 mesons. The non-prompt D^0-meson R_{AA} is significantly larger than the prompt one and the data are described by models that incorporate both collisional and radiative processes including a quark-mass dependence, and recombination in combination with fragmentation as a hadronization mechanism. Measurement of v_2 of non-prompt D^0 mesons is consistent with that from b-to-e v_2 and its non-zero value suggests that b quarks
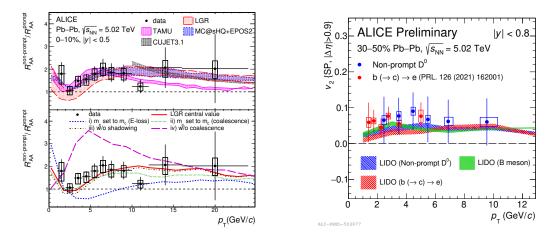
Figure 7: (Left) Non-prompt to prompt D^0-meson R_{AA} ratio as a function of p_T in central Pb–Pb collisions at $\sqrt{s_{NN}}$ = 5.02 TeV, compared to model predictions. Figure taken from [16]. (Right) Non-prompt D^0 v_2 compared with b-to-e v_2 and models in semi-central Pb-Pb collisions. Figure from [17].

partially thermalize in the medium or recombine with light quarks. More statistics is, however, needed to see to what extent c and b quarks participate differently to collective motion as hinted by differences in the data and to constrain spatial diffusion coefficient with beauty measurements.

Next, let us discuss interaction of jets with QGP. Although inclusive jet R_{AA} measurements suffer from limited sensitivity to discriminate between models, recent measurements highlighted here have a great potential to bring more insights. The first one is the measurement of the cone-size (R) dependence of the R_{AA}. The data reveal only a modest increase with jet radius and in fact, the R_{AA} never reaches unity even at jet $p_T \approx 1$ TeV [18]. The ratio of large and small radius jet R_{AA} sets significant constraints on models of jet quenching, medium response and wide angle radiation. Employing ML techniques, ALICE recently extended the measurements down to jet $p_T = 40$ GeV/c and larger R as shown in Figure 8. In this kinematic region, the background contamination is substantial, however this region is essential to constrain model predictions at LHC energy but also for comparison with RHIC.

Jet quenching is sensitive to the color charge and gluon-initiated jets are expected to lose more energy than quark ones. Although at the LHC the inclusive jet production is dominated by gluon-
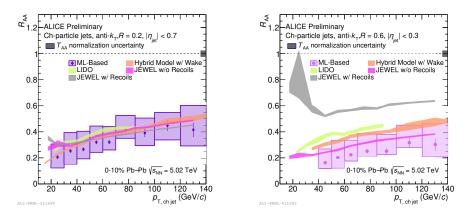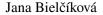

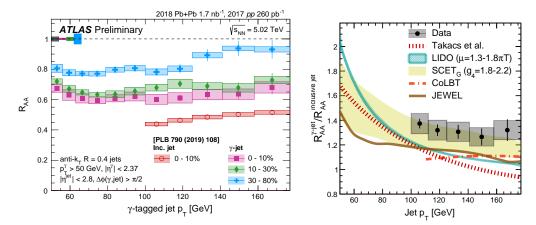**Figure 8:** Jet R_{AA} for R = 0.2 and 0.6 in central Pb-Pb collisions at $\sqrt{s_{NN}}$ = 5.02 TeV. Figures from [10].

Figure 9: The R_{AA} of γ-tagged jets as a function of jet p_T in Pb-Pb collisions at $\sqrt{s_{NN}} = 5.02$ TeV for different centrality classses. The inclusive jet R_{AA} in 0-10% events is shown for comparison. Figures taken from [19].

initiated jets, jets produced in association with an isolated γ are more likely to be initiated by a quark when compared to inclusive jets at the same p_T. The R_{AA} for γ-tagged jets measured by ATLAS is presented in Figure 9 (left) and is indeed significantly higher than that for inclusive jets. Although many calculations describe the inclusive jet R_{AA}, this new measurement sets new constraints on the color charge dependence of energy loss calculations. This is demonstrated by comparing the double R_{AA} ratio between γ-tagged and inclusive jets (cf. Figure 9 (right)). Calculations predict a value above unity, qualitatively in line with expectations, but the data are above most of the calculations with an exception of the SCET$_G$ calculation that describes the data within uncertainties.

Semi-inclusive measurements of jets recoiling from a high-momentum hadron or photon give access to energy transported to angles larger than the jet radius and ratios of yields at different R values enable measurements of medium modification of jet shape (intra-jet broadening). The inter-jet broadening and related acoplanarity can be approached via azimuthal distributions of recoiling jets relative to the trigger particle. The acoplanarity of lower energy jets is predicted to be sensitive
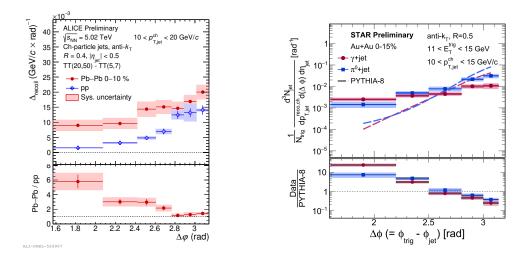

Figure 10: Azimuthal distribution of jets recoiling from: a hadron in central Pb-Pb collisions and pp collisions at $\sqrt{s_{NN}} = 5.02$ TeV measured by ALICE (left) [20] and from a π^0 and direct γ in Au-Au collisions at $\sqrt{s_{NN}} = 200$ GeV measured by STAR (right) [21].
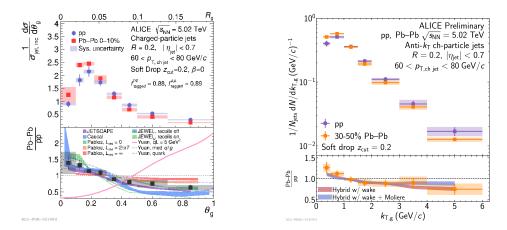
7

Figure 11: (Left) θ_g distributions for jets in pp and 0-10% central Pb-Pb collisions at $\sqrt{s_{NN}}$ = 5.02 TeV for R = 0.2. Figure taken from [22]. (Right) Comparison of the hardest k_T jet splitting using Softdrop grroming for R = 0.2 jets in pp and 30-50% central Pb-Pb collisions at $\sqrt{s_{NN}}$ = 5 TeV. Figure taken from [20].

to the jet transport parameter in medium and the path-length traversed by a parton in the medium. Perhaps the most interesting application of this analysis method are searches for enhanced jet yield in the tail of the $\Delta\phi$ distribution that could originate from medium-induced Molière scattering of quasi-particles in the QGP displayed in Figure 10. Within uncertainties, no sign of quasi-particles is detected and more statistics is needed to provide definite conclusion.

Jet substructure provides a multi-scale probe of QCD and can help to improve understanding of hadronization mechanisms and the nature of jet quenching. Grooming techniques must be applied on reconstructed jets to reduce non-perturbative effects by removing soft large-angle radiation (e.g. via SoftDrop). While no significant in-medium modification of the groomed jet momentum splitting fraction (z_g) distribution has been observed, the groomed jet radius (θ_g) manifests a narrowing in Pb–Pb compared to pp collisions as can be seen in Figure 11. This observation provides direct evidence of the modification of the angular structure of jets in the QGP. Recently a new family of so-called 'dynamical groomers' has been introduced [23] which reduces the number of unconstrained parameters and could offer a larger discriminating power than SoftDrop as the fluctuating background in heavy-ion collisions makes the reconstruction of groomed jet observables challenging. Figure 11 (right) shows the first measurement of dynamically groomed k_T by ALICE. Deflections off scattering centers are expected to increase the relative k_T of subjets within a jet in Pb-Pb compared to pp collisions. Within current uncertainties, the data are consistent with no modification at high k_T and a hint of modification at low k_T.

4. Quarkonia as a QGP thermometer

In the QGP, quarkonia are expected to be suppressed by Debye screening or dissociated, but the presence of QGP could also lead to enhanced quarkonia production by recombination processes of uncorrelated c and $\bar{c}$ quarks, especially at the LHC energies due to the large increase of the $c\bar{c}$ production cross-section. Differences in the binding energies of individual quarkonium states lead to a sequential melting of the quarkonia states with increasing temperature of the medium and hence quarkonia are commonly considered as a 'QGP thermometer'.
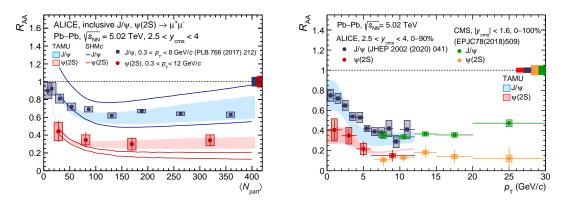
Figure 12: R_{AA} for the $\psi(2S)$ and J/ψ as a function of centrality (left) and p_T (right) by ALICE and CMS compared with models. Figure taken from [10].

As suppression and regeneration in medium act in opposite directions, it is important to study different charmonium states to learn about the relative strength of these two mechanisms. Figure 12 shows the R_{AA} of J/ψ and $\psi(2S)$ measured by ALICE and CMS in Pb-Pb collisions at $\sqrt{s_{NN}}$ = 5.02 TeV. Data reveals a stronger suppression for $\psi(2S)$ compared to J/ψ, as expected. At low p_T, an increase of R_{AA} is observed, in line with a significant role of regeneration. The transport model (TAMU) which includes recombination of c quarks in QGP, reproduces the data better than statistical hadronization approach (SHMc). As the number of $b\bar{b}$ pairs in a collision is much smaller than for c quarks, bottomonia are a cleaner probe because they are almost unaffected by the recombination. CMS has observed for the first time the $\Upsilon(3S)$ meson in central Pb-Pb collisions, completing the pattern of sequentail suppression of bottomonium states in QGP. The suppression of all Υ states displayed in Figure 13 is found to be stronger for $\Upsilon(3S)$ compared to $\Upsilon(2S)$ and $\Upsilon(1S)$ states. These results provide new constraints on models describing the dynamics of quarkonia in the QGP.
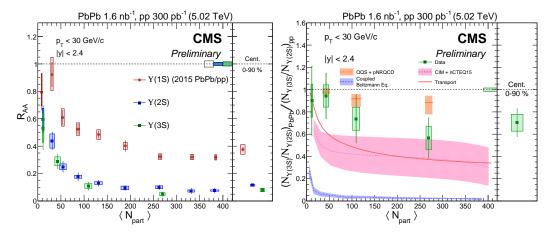

Figure 13: (Left) The R_{AA} for the $\Upsilon(1S)$, $\Upsilon(2S)$, and $\Upsilon(3S)$ mesons as a function of Pb-Pb collision centrality. (Right) The double ratio of $\Upsilon(3S)/\Upsilon(2S)$. Figures taken from [24].

5. Outlook

Experimental studies of heavy-ion collisions are now entering a new era of microscopic studies of the QGP thanks to upgraded LHC experiments, including the fixed-target program SMOG at

LHCb. At BNL, STAR upgraded with forward detectors and a new sPHENIX experiment will collect in 2023-25 unprecedented statistics to complete the 25 years RHIC mission of dedicated QGP and QCD phase diagram studies.

References

[1] H. Zbroszczyk *et al.* (STAR Collaboration), PoS(ICHEP2022)495

[2] R. Aaij *et al.* (LHCb Collaboration), Phys. Rev. Lett. **128** (2022) 142004

[3] LHCb Collaboration, arXiv: 2204.10608

[4] Y. Shi, L. Wang, S.-Y. Wei, B.-W. Xiao, Phys. Rev. Lett. **128** (2022) 202302

[5] R. Aaij *et al.* (LHCb Collaboration), JHEP **10** (2017) 090

[6] R. Abdul Khalek *et al.*, Eur. Phys. J. C **82** (2022) 507

[7] M. Klasen *et al.*, PoS(ICHEP2022)443

[8] ALICE Collaboration, arXiv: 2206.04587

[9] P. Dixit *et al.* (STAR Collaboration), PoS(ICHEP2022)496

[10] A. Dainese *et al.* (ALICE Collaboration), PoS(ICHEP2022)008

[11] CMS Collaboration, CMS-PAS-HIN-21-008

[12] S. Acharya *et al.* (ALICE), Phys. Rev. D **105** (2022) L011103; PoS(ICHEP2022)764

[13] S. Acharya *et al.* (ALICE Collaboration), Phys. Lett. B **827** (2022) 136986

[14] J. Adam *et al.* (STAR Collaboration), Phys. Rev. Lett. 124 (2020) 172301

[15] S. Acharya *et al.* (ALICE Collaboration), arXiv: 2112.08156

[16] S. Acharya *et al.* (ALICE Collaboration), arXiv: 2202.00815

[17] B. Zhang *et al.* (ALICE Collaboration), PoS(ICHEP2022)449

[18] A. M. Sirunyan *et al.* (CMS Collaboration), JHEP **05** (2021) 284

[19] ATLAS Collaboration, ATLAS-CONF-2022-019

[20] R. Ehlers *et al.* (ALICE Collaboration), PoS(ICHEP2022)460

[21] D. Anderson *et al.* (STAR Collaboration), PoS(ICHEP2022)500

[22] S. Acharya *et al.* (ALICE Collaboration), Phys. Rev. Lett. **128** (2022) 102001

[23] Y. Mehtar-Tani, A. Soto-Ontoso, K. Tywoniuk, Phys. Rev. D **101** (2020) 034004

[24] CMS Collaboration, CMS-PAS-HIN-21-007